

Taylor & Francis
Taylor & Francis Group

Journal of Biomolecular Structure and Dynamics

ISSN: (Print) (Online) Journal homepage: https://www.tandfonline.com/loi/tbsd20

In silico molecular modeling and simulations of black tea theaflavins revealed theaflavin-3'-gallate as putative liver X receptor-beta agonist

Temidayo O. Adigun, Ammar U. Danazumi, Haruna I. Umar, Asiat Na'Allah, Mutiu A. Alabi, Wisdom O. Joel, Adepeju Aberuagba, Omokolade O. Alejolowo, Joy O. Bamidele, Olakunle S. Omotayo & Oluwatobi A. Medayedupin

To cite this article: Temidayo O. Adigun, Ammar U. Danazumi, Haruna I. Umar, Asiat Na'Allah, Mutiu A. Alabi, Wisdom O. Joel, Adepeju Aberuagba, Omokolade O. Alejolowo, Joy O. Bamidele, Olakunle S. Omotayo & Oluwatobi A. Medayedupin (2023): In silico molecular modeling and simulations of black tea theaflavins revealed theaflavin-3'-gallate as putative liver X receptor-beta agonist, Journal of Biomolecular Structure and Dynamics, DOI: 10.1080/07391102.2023.2175264

To link to this article: https://doi.org/10.1080/07391102.2023.2175264

Published online: 02 Feb 2023.

Submit your article to this journal

Article views: 158

View related articles

View Crossmark data

Full Terms & Conditions of access and use can be found at
https://www.tandfonline.com/action/journalInformation?journalCode=tbsd20

JOURNAL OF BIOMOLECULAR STRUCTURE AND DYNAMICS
https://doi.org/10.1080/07391102.2023.2175264

Taylor & Francis
Taylor & Francis Group

Check for updates

In silico molecular modeling and simulations of black tea theaflavins revealed theaflavin-3′-gallate as putative liver X receptor-beta agonist

Temidayo O. Adigun[a], Ammar U. Danazumi[d,e], Haruna I. Umar[b,c], Asiat Na'Allah[f], Mutiu A. Alabi[f], Wisdom O. Joel[g], Adepeju Aberuagba[h], Omokolade O. Alejolowo[i], Joy O. Bamidele[j], Olakunle S. Omotayo[j] and Oluwatobi A. Medayedupin[a]

[a]Department of Biochemistry, Faculty of Life Sciences, University of Ilorin, Ilorin, Nigeria; [b]Molecular Biology and Bioinformatics Lab, Department of Biochemistry, Federal University of Technology Akure, Akure, Nigeria; [c]Computer-aided Therapeutic Discovery and Design Group, Federal University of Technology Akure, Akure, Nigeria; [d]Faculty of Chemistry, Warsaw, University of Technology, Warsaw, Poland; [e]Groningen Research Institute of Pharmacy, University of Groningen, Groningen, The Netherlands; [f]Department of Biochemistry, Faculty of Pure and Applied Sciences, Kwara State University, Malete, Nigeria; [g]Department of Biochemistry, College of Science and Technology, Covenant University, Ota, Nigeria; [h]Department of Biochemistry, McPherson University, Seriki Sotayo, Nigeria; [i]Department of Biochemistry, Landmark University, Omu-Aran, Nigeria; [j]Science Laboratory Technology, The Federal Polytechnic Ilaro, Ilaro, Nigeria

Communicated by Ramaswamy H. Sarma

ABSTRACT

The low constitutive activation of Liver X receptor, an endogenous nuclear receptor with two subtypes (α and β), is a condition lying at the crossroad of cancer and cardiovascular disease. Both natural and synthetic Liver X receptor agonists have reportedly shown remarkable antiproliferative and atheroprotective effects but the repeated doses of its synthetic ones are also paradoxically associated with hyperlipidaemic effects and neurotoxicity, though attributed to the alpha subtype. This highlights the need for novel, safe, and potent LXR-beta-selective agonists. Hypocholesterolaemic effects of black theaflavins have been widely reported, but data on the exact theaflavin compound (s) responsible for these effects is currently lacking. Neither is information on the possible modulatory effects of the compound (s) on LXR-beta nor its possible implications in the context of drug development for cardiovascular diseases and cancers is explored. On this account, we investigated the potential interaction of four main theaflavin monomers (TF1, TF2A, TF2B & TF3) with human LXR-beta through robust computational modelling that entails molecular docking, free energy calculations and molecular dynamics simulations. The ligands were further profiled (*in silico*) for absorption, distribution, metabolism, excretion, and toxicological properties. Our result revealed theaflavin TF2B as a putative LXR-beta agonist, possibly responsible for the widely observed hypocholesterolaemic effect in black tea. This finding, while encouraging, needs to be experimentally verified in wet studies.

ARTICLE HISTORY
Received 12 November 2022
Accepted 11 January 2023

KEYWORDS
Liver X receptor-beta; theflavins; black tea; theaflavin-3′-gallate; hypocholesterolaemia

1. Introduction

Liver X receptors (LXRs) are endogenous oxysterols-activating nuclear receptors, with α isoform (located on human chromosome 11p11.2) and β isoform (located on human chromosome 19q13.3) (Nguyen-Vu et al., 2013; Viennois et al., 2011; Zhao & Dahlman-Wright, 2010). They have both been characterized as being transcriptionally active (by forming heterodimers with 9-cis retinoic acid receptors) when the oxysterols (such as 22(R)-hydroxycholesterol, 24(S),25-epoxycholesterol, etc.) and cholesterol precursors (such as desmosterol (PubChem ID: 439577), etc.) binds to them (Beltowski, 2008; Schulman, 2017). They however differ from conventional steroid receptors in that they show low constitutive activation in the absence of ligand, despite the fact they play critical roles in the reverse cholesterol transport (RCT) pathway, from decreased intestinal cholesterol uptake to cellular cholesterol efflux (via ABCA1 and ABCG1 transporters) to high-density lipoprotein metabolism to biliary cholesterol excretion (via ABCG5 and ABCG8 transporters) (Bradley & Tontonoz, 2005; Lund et al., 2003). The LXR-α has been shown as highly expressed in metabolically active tissue subsets including the liver, adipose tissue, small intestine, spleen, kidney, heart, lung, and skeletal muscle, while the LXR-beta is ubiquitously expressed throughout the human body (Repa et al., 2002; Shao et al., 2021). They function as cholesterol-sensing inducers of genes preventing overload of cellular cholesterol through these pathways (Shao et al., 2020; Zhao & Dahlman-Wright, 2010), while their low expressions have been shown to characterize a wide range of cardiovascular diseases (CVDs); a prominent (along with cancer) cause of current global morbidity and mortality rates (Kick et al., 2016; Nguyen-Vu et al., 2013).

The ability of LXRs, therefore, to promote macrophage cholesterol efflux and advance the RCT pathway has established the scientific interest in the therapeutic potential of LXR ligands for CVDs therapy, while the discovery, however, of hyperlipidaemic effects of LXR-alpha agonists and the

CONTACT Temidayo O. Adigun prothesis4life@gmail.com; 07-55eh245pg@students.unilorin.edu.ng
© 2023 Informa UK Limited, trading as Taylor & Francis Group

atheroprotective sufficiency of sole LXR-beta activation has increased the search for safe and potent LXR-beta-selective agonists (Schulman, 2017).

Cancer cells, on the other hand, have been shown to frequently gain selective proliferation via increased low-density lipoprotein (LDL) receptor-mediated uptake of exogenous cholesterol as well as characterized by mutated or dysregulated forms of genes involved in cholesterol homeostasis (Kick et al., 2016; Schulman, 2017). Thus, the same resultant conditions stemming from low LXR activation (i.e. high intracellular cholesterol level due to increased *de novo* synthesis, and reduced ABC transporters-mediated efflux) have been shown to sustain the metabolic needs and proliferation capacity of various cancer subtypes (Morrow et al., 2010; Zeng et al., 2012).

Also, evidence is linking low LXRs expression levels to diverse cancer subtypes via other mechanisms such as activity reduction of cell cycle regulators (including S-phase kinase-associated protein (SPK2), cyclin-dependent kinases, etc.) (Chu et al., 2006; Repa et al., 2000), apoptosis inhibition (Vedin et al., 2009), lipid rafts-associated compartmentation of vascular endothelial growth factor receptor-2 in angiogenesis and its consequential metastasis (Ju et al., 2017). Therefore, it is no longer a surprise that LXR is being considered a highly druggable target for the potential treatment of a wide variety of cancers (Ju et al., 2017; Lin & Gustafsson, 2015). The LXR agonists (both natural and synthetic) have reportedly been shown to display remarkable antiproliferative effects against cancer via intracellular cholesterol depletion (Villa et al., 2016; Bovenga et al., 2015), with broad-spectrum activity via receptor tyrosine kinases (including epidermal growth factor receptor, vascular endothelial growth factor receptor 2, protein kinase B, phosphoinositide 3-kinase etc.) inhibitions (Noghero et al., 2012; Shao et al., 2021; Wang et al., 2019) as well as increased tumour suppressing p53 levels in cancer cell lines (Vedin et al., 2009).

Long et al. (2018) discovered a positive link between LXR expression and improved HCC survival (Long et al., 2018), while Vázquez-S algado et al. (2019) showed the activity boost of sorafenib by LXR agonist against hepatocellular carcinoma cells (Vázquez-S algado et al., 2019).

The challenge remains, however, that antiproliferative activities of repeated doses of currently developed synthetic LXR agonists are also usually accompanied by increasing low-density lipoprotein cholesterol and triglycerides, as demonstrated in hamsters and cynomolgus monkeys (Groot et al., 2005; Kick et al., 2016), though this observed hyperlipidaemic effects may have stemmed from the alpha subtype of the protein as reported by Schulman (2017) (Schulman, 2017), which necessitates the search for safe and potent LXR-beta-selective agonists and formed the rationale for this study. The LXR agonists are also associated with neurotoxicity (Kick et al., 2016).

The most widely consumed beverage in the whole world is tea (*Camellia sinensis*). The drinks being derived from it is second only to water in consumption (Jin et al., 2013; Ramadan et al., 2009). Tea, depending on the processing methods, is of diverse variants, including black tea, green tea (unfermented), and oolong tea (fully fermented), and are known to produce diverse chemical compositions with varying nutritional and therapeutic efficacies (Ramadan et al., 2009).

These have been shown to be rich in antioxidant polyphenols (including thearubigins, flavonols, catechins, and theaflavins) which contain the vicinal or trihydroxy structure responsible for the free radicals-chelating effect (Jin et al., 2013; Ramadan et al., 2009) while, in addition, theaflavins are known to contain electron-donating benzotropolone moiety (Jin et al., 2013). These antioxidant properties have always been referenced as the most significant therapeutic benefits of tea until recent times in which several reported experimental animal models and epidemiological studies have shown an inverse relationship between the consumption of tea and plasma cholesterol levels (Maron et al., 2003; Trautwein et al., 2010).

Specifically, the theaflavins in black tea (being produced by condensation of quinones; the oxidation products of catechins (tea tannins) by polyphenol oxidase) have been shown to deplete intestinal cholesterol absorption through inhibition of dietary mixed micelle formation, reduce plasma triglycerides, cholesterol, and LDL cholesterol through elevated faecal lipid excretion in animal models of hypercholesterolaemia (Maron et al., 2003; Ramadan et al., 2009), suppresses lipogenesis through fatty acid synthase inhibition (Jin et al., 2013), inhibits pancreatic lipase and lipoprotein lipase expression (Jin et al., 2013), reduce hepatic cholesterol accumulation (Lin et al., 2007), as well as inhibits synthesis of cholesterol through upregulated liver LDL receptor expression (Kuo et al., 2005; Ramadan et al., 2009).

Jin et al. (2013) reported that the four theaflavin monomers consisting of Theaflavin (TF1) (PubChem ID: 135403798), theaflavin-3-gallate (TF2A) (PubChem ID: 169167), theaflavin-3′-gallate (TF2B) (PubChem ID: 135625500), and theaflavin-3,3′-digallate (TF3) (PubChem ID: 440069529) are the major theaflavins constituting black tea (Jin et al., 2013).

There is not yet any published data, however, on the exact theaflavin compound (s) being responsible for the widely observed anti-hypercholesterolaemic effects of black tea. Neither is there any information on the possible modulatory effects of the compound (s) on LXR-beta and its possible implications in the efforts to develop novel potent and safe drugs for the treatment of cardiovascular diseases and cancers.

This study, therefore, aims, through molecular modeling, to establish whether the possible modulatory effect of any of the reported black tea theaflavin compounds on LXR-beta can be established, the exact compound (s) involved, as well as the implication (s) in hypercholesterolemia-associated cancer conditions.

2. Methods

2.1. Protein preparation

The PDB coordinate files (PDB ID: 6S4T) of the crystal structure of human (*Homo sapiens*) Liver X receptor beta isoform (LXR-beta) were retrieved from the protein data bank (http://

www.rcsb.org) and prepared using the protein preparation wizard of Schrodinger maestro v 12.5.139. Briefly, the co-crystalized KVB compound was deleted, while the protein chain was prepared at the OPLS2005 force field under a pH of 7.02.0. All steric clashes were removed, hydrogen bond order was restored, and the missing side chains and loops were replaced with prime. Water molecules with a molecular weight greater than 5.00 and fewer than three hydrogen bonds to non-waters were deleted from the ionized (Het) groups, while bond orders were assigned. This was energetically minimized at the polarity charge cutoff set at 0.25.

2.2. Ligand preparation

The two-dimensional structures of the four theaflavins (TF1 (PubChem ID: 135403798), TF2A (PubChem ID: 169167), TF2B (PubChem ID: 135625500), and TF3 (PubChem ID: 440069529) compounds, as well as desmosterol (PubChem ID: 439577), were retrieved from the PubChem database and prepared using the Schrodinger maestro ligand preparation wizard, in which the ligands were desalted, possible Epik states and tautomers were generated at the target pH of 7.02.0, and then subjected to energy minimization under OPLS2005 force field through the MacroModel wizard.

2.3. Receptor grid generation

The co-crystallized ligand was separated from the active site of the receptor chain using the defined receptor. The atoms had Van der Waals radii of 1.0 ångström and partial atomic charges of less than 0.25 ångström by default. The active site is represented by an enclosing box at the workspace centroid of selected residues around the co-crystallized ligands while, using the default Glide settings, a grid centered on the ligand was generated using this protocol. All ligands were docked into this grid structure in this study.

2.4. Glide standard precision docking and molecular Mechanics-Generalized born surface area calculations

Glide standard precision docking was used to dock a sampled flexible ligand (based on nitrogen inversion and ring conformations) into the target receptor grid, and post-docking minimization was performed. The docking score was calculated using input partial charges, while ligands with more than 500 atoms were not docked or scored. The van der Waals radii of ligand atoms with partial atomic charge were scaled by 0.80 compared to the partial charge cut-off of 0.15, and the Epik state penalties were added to the docking score.

Prime was also used to calculate the molecular mechanics generalized Born surface area free energy change (MMGBSA dG) of the docked ligands using the VSGB solvation model and the input ligand partial charges. The flexible residues were constrained, and the energy calculations were carried out using all processed ligands, while more precise and flexible docking was also performed on the defined receptor grid using the Glide extra precision (XP) feature.

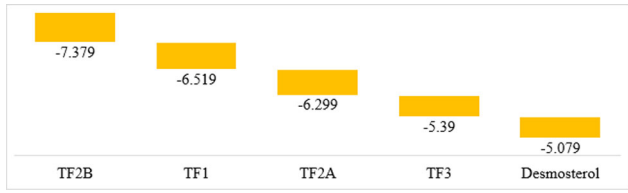


Figure 1. Glide standard precision GScores of binding compounds to liver X receptor-beta.

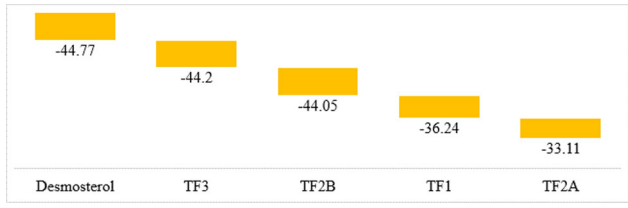


Figure 2. Molecular mechanics – generalized born surface area values of binding compounds to liver X receptor-beta following glide standard precision docking.

2.5. Glide quantum polarized ligand docking

The initial Glide docking ligand charges were generated using the standard semiempirical method precision, in which the pose was discarded as duplicate if the root mean square deviation was less than 0.5 ångström and the maximum atomic displacement was less than 1.3. Before redocking at standard precision, the quantum mechanics charges for free ligands in the gas phase were calculated using the Coulson charge semi-empirical method. Ligands with the best binding pose were finally chosen based on the Glide Score, while the van der Waals scaling for the receptor and ligand was 1.0 and 0.8, respectively.

2.6. Glide induced fit docking

The maximum of 20 different poses, by default, of each ligand were generated through standard protocol at the OPLS 3e forcefield of the induced fit docking module. These were docked with Glide Standard precision in which the ring conformations of the ligands were sampled at the energy window of 2.5 Kcal/mol, the planarity of conjugated Pi groups was enhanced, and the nonplanar conformations of amide bonds were penalized. The receptor and ligand van der Waals scaling were set at the default value for best-docked ligand pose allowance (0.50), while the residues within 5.0 Å of ligand poses were refined, with their side chains optimized. The ligands within 30.0 Kcal/mol of the best structure within top 20 of overall initially docked structures, as well as Coulomb-van der Waals score of 100 and hydrogen bond score of 0.05 were retained. These were then redocked with Glide extra precision into the refined structure for final binding energy score calculation (IFDScore) and ranking of the output poses.

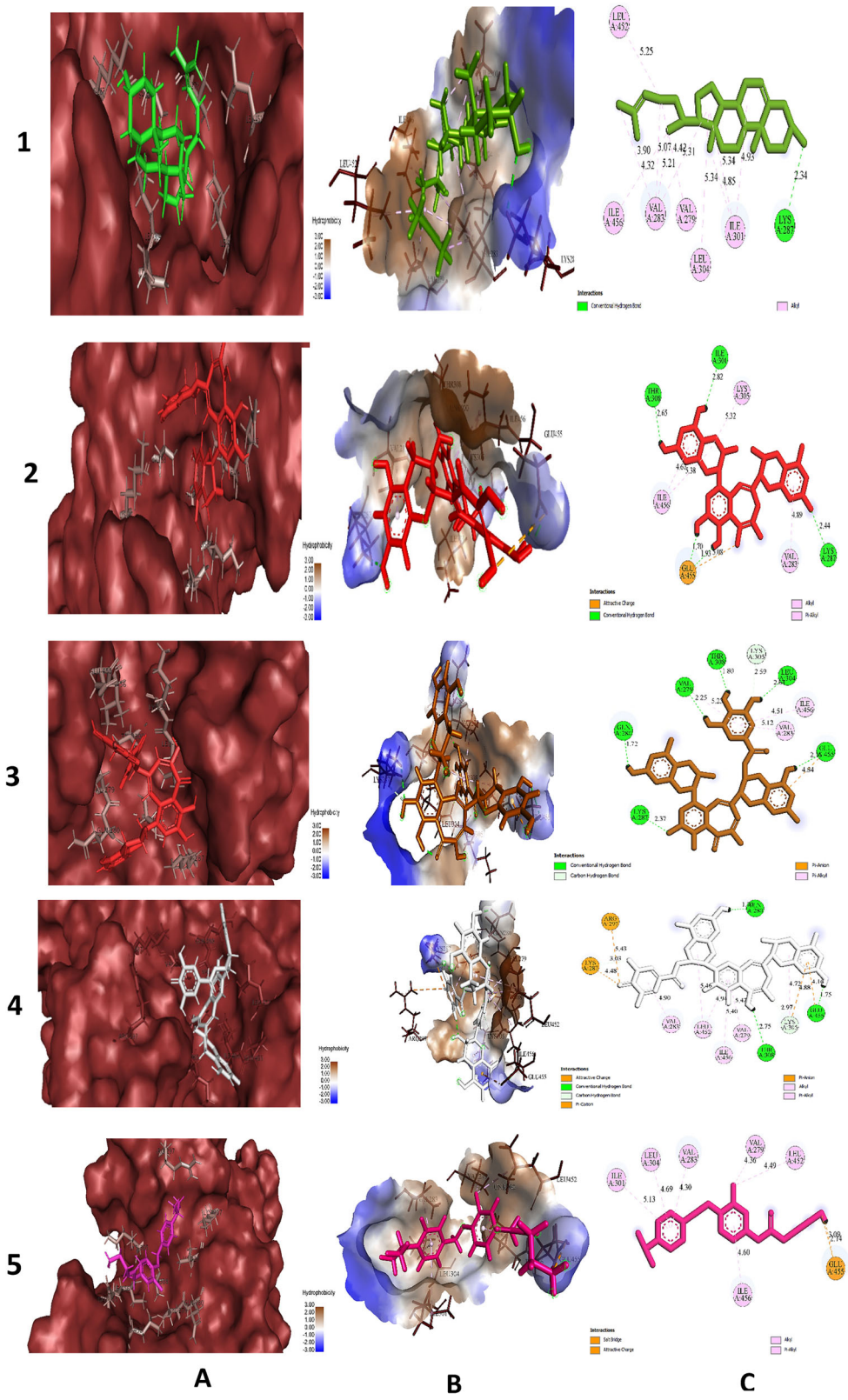


Figure 3. Pocket view (A), pocket hydrophobicity (B) and two-dimensional view (C) of binding interactions between liver X receptor-beta and desmosterol (1), TF1 (2), TF2A (3), TF2B (4) and TF3 (5) following glide standard precision docking of the compounds.

2.7. Protein-ligand interaction analysis

The Glide merging procedure was used to create the docked ligands in complex with the targets and their corresponding binding poses. The BIOVIA discovery studio suite was used to visualize the two-dimensional interactions between the ligands and the target binding pocket residues, and PyMol® was used to represent the active pocket view of interactions. The Glide ligand interaction 2D visualizer was also employed for post-induced fit docking protein-ligand visualization.

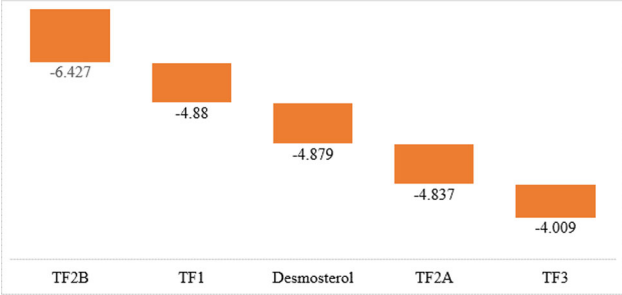


Figure 4. Glide extra precision GScores of binding compounds to liver X receptor-beta following quantum polarized ligand docking.

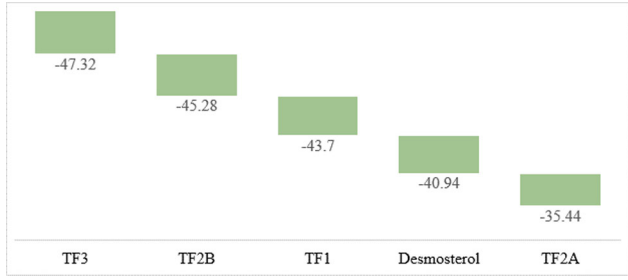


Figure 5. Molecular mechanics – generalized born surface area values of binding compounds to liver X receptor-beta following quantum polarized ligand docking.

2.8. Normal mode - coarse grained simulation analysis of target protein

The deformability, B-factor, covariance matrix, main chain deformability plot, B-factor values, eigen value, as well as elastic network model of the apo protein as well as the hit compound-protein complex were simulated from their internal coordinates using the online-based iMOD software (López-Blanco et al., 2014).

2.9. Atomistic molecular dynamic simulations of protein complexes

Docked protein-ligand complexes were used to prepare topology for MD simulation using CHARMM all-atom force field and CGenFF for protein and ligand respectively (Vanommeslaeghe et al., 2010; Yu et al., 2012). The systems were energetically minimized for 5000 steps and equilibrated to a temperature of 300 K and pressure of 1 atm in NVT and NPT ensembles for 100 picoseconds each. This was followed by final MD run for the duration of 100 ns each in the NPT ensemble. The GROMACs 2021 simulation engine was employed for the simulation runs in which parameters such as root mean square deviation (RMSD), radius of gyration (Rg), root mean square fluctuations (RMSF) and solvent-accessible surface area (SASA) were calculated from generated trajectories. All graphs were plotted using the Python matplotlib library.

2.10. In-silico pharmacokinetics and toxicity profiling

The resultant hit compound from this study was profiled for its absorption, distribution,

metabolism, excretion, and toxicity properties by submitting its structure description file coordinates for evaluation by the algorithms of web-based ProTOX-II (Prediction of TOXicity of chemicals) and SwissADME (http://www.swissadme.ch/index.php), OSIRIS Data Warrior v5.5.0 chemical properties calculator, and Glide QikProp evaluator.

3. Results and discussion

3.1. Standard precision docking of theaflavins

Binding affinity is usually considered to be a priority in the selection of the best candidate, via virtual screening, for high throughput tests in drug discovery, as it helps predetermine the modulatory potential of the screened compound, via the binding effect, on the target protein (Chen, 2015). The four theaflavin compounds (TF1, TF2A, TF2B, TF3) displayed higher Glide GScores than that of desmosterol (-5.079 Kcal/mol) (as shown in Figure 1), with the TF2B having the highest binding score. Desmosterol (-44.77 Kcal/mol), however, displayed the highest molecular mechanics generalized Born surface area (MMGBSA) value than the theaflavin compounds with TF3 (-44.2 Kcal/mol) and TF2B (-44.05 Kcal/mol) having the closest values to that of the standard (as shown in Figure 2). The free energy calculations of the theaflavin compounds, thus, revealed the theaflavin TF3 and TF2B compounds as the closest hits comparable to that of standard in this study post-Glide docking procedure.

3.2. Ligand-protein interactions following standard precision docking of theaflavins

The TF1 binds in common with the desmosterol, through the hydrophobic alkyl bond, to valine 283, and isoleucine 456 (which is at close proximity to the hydrophobic LXR-beta H12 region; a key agonistic region of the protein), as well as the lysine 305, of the liver X receptor-beta protein at the bond distances of 5.32 ångström, 4.89 ångström, and 5.03 ångström (Figure 3C; 2). It also binds through the conventional hydrogen bond to threonine 308, isoleucine 301, and lysine 287 respectively at the bond distance of 2.65 ångström, 2.82 ångström, 2.44 ångström respectively. This is also in addition to bonding of the compound to glutamic acid 455 of the protein through the conventional hydrogen bond at a distance of 1.82 ångström and a rare attractive charge at the bond distance of 1.82 ångström. This also suggests the stronger binding potential of the TF1 compound to the desmosterol-binding site of the LXR-beta protein.

The TF2A binds to glutamine 280, lysine 287, threonine 308, leucine 304, valine 279, glutamic acid 455 through the conventional hydrogen bond respectively at the distances of 1.72 ångström, 2.37 ångström, 1.80 ångström, 2.64 ångström, 2.25 ångström, 2.16 ångström in addition to the binding of the compound through the carbon-hydrogen bond to lysine 305 at the distance of 2.59 ångström; valine 279, isoleucine 456 and valine 283 through the hydrophobic Pi-alkyl bond at the bond distance of 5.23, 4.51, and 5.12 ångström respectively, as well as glutamic acid 455 through the hydrophobic Pi-Anion bond at 4.84 ångström (Figure 3C; 3).

The theaflavin compound TF2B binds to valine 283, isoleucine 456, valine 279, and leucine 452 respectively at the

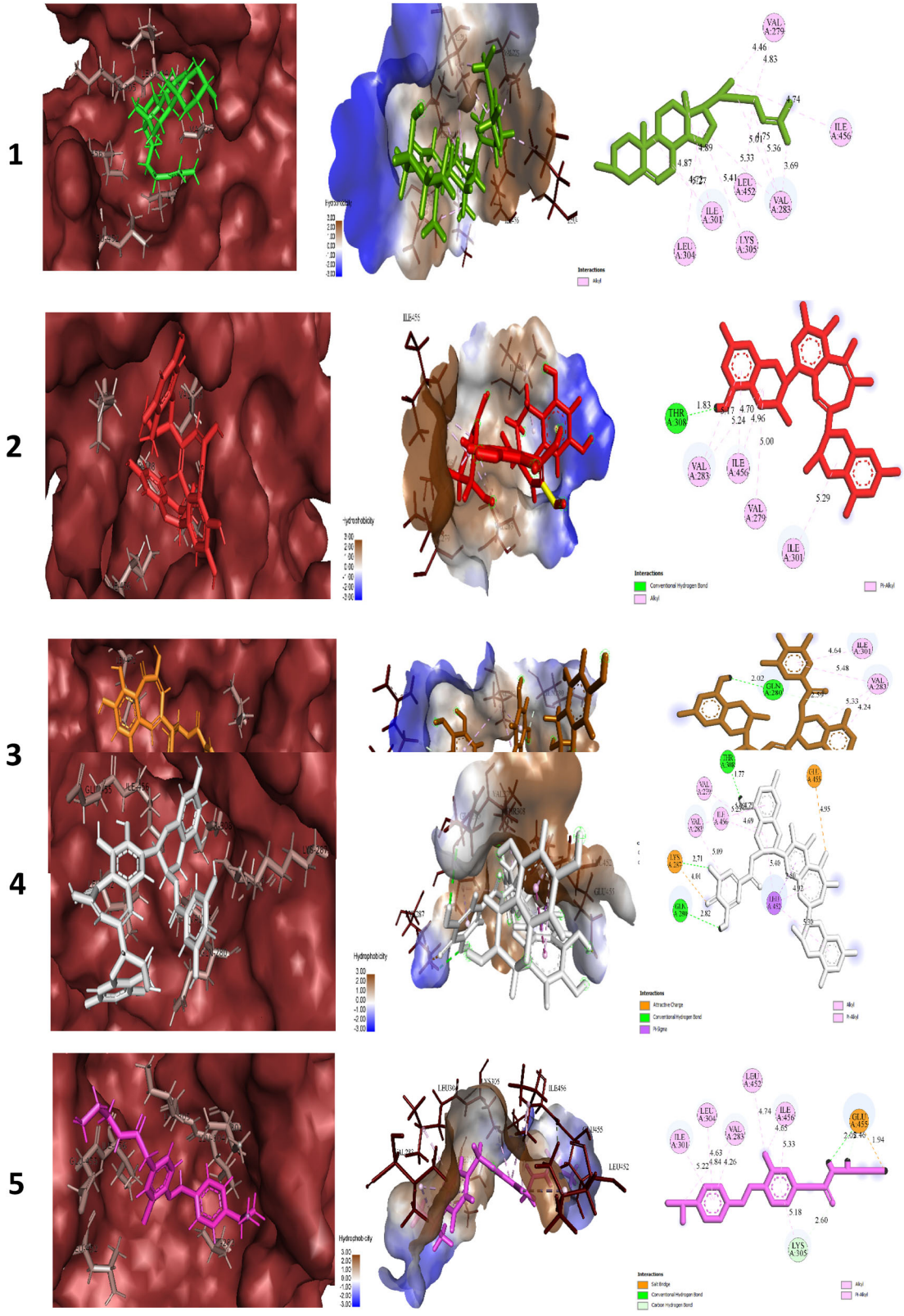


Figure 6. Pocket view (A), pocket hydrophobicity (B) and two-dimensional view (C) of binding interactions between liver X receptor-beta and desmosterol (1), TF1 (2), TF2A (3), TF2B (4) and TF3 (5) following quantum polarized ligand docking of the compounds.

bond distances of 4.90 ångström, 5.40 ångström, 5.42 ångström, and average bond distance of 5.2 ångström through the hydrophobic alkyl bond, in addition to binding of the compound respectively through conventional hydrogen bond to glutamine 280, glutamic acid 455, threonine 308 of the protein at the distances of 1.70 ångström, 1.75 ångström, 2.75 ångström (Figure 3C; 4).

Compound TF2B also binds to lysine 305 through the hydrophobic Pi-anion and Pi-Alkyl bonds at the average distance of 4.8 ångström in addition to carbon-hydrogen bond

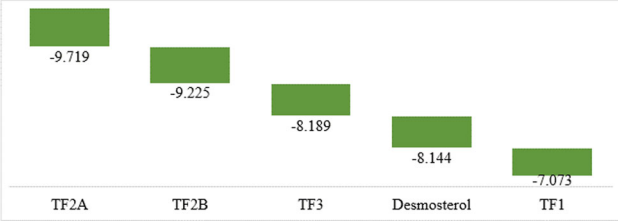


Figure 7. Induced fit docking gscores of binding compounds to liver X receptor-beta.

at the distance of 2.97 ångström. It also binds to arginine 297 of the protein through Pi-anion bond at a distance of 5.43 ångström, as well as lysine 287 through the Pi-Cation and Carbon-Hydrogen bond at the distances of 4.48 and 3.03 ångström respectively, while the TF3 compound binds through the hydrophobic alkyl and Pi-alkyl bonds to isoleucine 301, leucine 304, valine 283, valine 279, and isoleucine 456 at the distances of 5.13, 4.69, 4.30, 4.36, and 4.60 ångström respectively as well as glutamic acid 455 through a rare attractive charge and a salt bridge at the bond distances of 3.09 and 2.14 ångström respectively (Figure 3C; 5).

The theaflavin compounds, therefore, binds to the various LXR-beta protein functional residues, including leucine 452, valine 283 and 279, as well as lysine 287, thereby revealing the modulatory potentials of the compounds against the LXR-beta protein target.

3.3. Quantum polarized ligand docking of theaflavins

The QM-polarized ligand docking replaces the resultant charges of quantum mechanical calculations on ligands in the receptor field to enhance the partial charges on ligand atoms in a Glide docking run, thereby accounting for polarization of the ligand charges by the receptor, while redocking of the ligands with the resultant new charges can result in improved docking accuracy.

The TF2B (-6.427 Kcal/mol) and TF1 (-4.880 Kcal/mol) compounds exhibited higher Glide GScores than Desmosterol (-4.879 Kcal/mol) following quantum polarized ligand docking in this study, while the compound with the least value is TF3 (-4.009 Kcal/mol) (Figure 4).

The MMGBSA values of the theaflavin compounds, except the TF2A (- 35.44 Kcal/mol), were however higher than that of desmosterol (-40.94 Kcal/mol), with the TF3 compound displaying the highest energy value of −47.32 Kcal/mol (Figure 5).

3.4. Ligand-protein interactions following quantum polarized ligand docking of theaflavins

The discovery of novel compounds with effective interactions to the target receptor, with its consequential high likelihood of potency in *vivo*, entails optimizing the structure interactions with the target (Patrick, 2013), as observed in the improved docking pose by the receptor-ligand polarization in this study.

The TF1 compound binds to threonine 308 of the protein through the conventional hydrogen bond at the distance of 1.83 ångström, as well as valine 279 and isoleucine 301, in common with desmosterol binding, through the hydrophobic alkyl bond at the distances of 5.00 and 5.29 respectively. This is in addition to binding of the compound to valine 283 and isoleucine 456 of the protein through the hydrophobic Pi-Alkyl at the average bond distances respectively of 5.21 and 4.83 ångström respectively, following quantum polarized ligand docking (Figure 6C; 2).

The TF2A compound also binds to isoleucine 301 and valine 283 in common with that of desmosterol through the hydrophobic alkyl bond at the distance of 4.64 ångström and the average distance of 5.02 ångström respectively, glutamine 280 through the conventional hydrogen bond at the distance of 2.02 ångström, as well as leucine 452 through the hydrophobic Pi-alkyl and hydrophilic carbon-hydrogen bond respectively at the bond distances of 3.87 ångström and 2.86 ångström (Figure 6C; 3).

The TF2B binds to leucine 452 through the Pi-Sigma bond at the average distance of 3.71 ångström, glutamic acid 455 through a rare attractive charge at the distance of 4.95 ångström, threonine 308 and glutamine 280 through the conventional hydrogen bond at 1.77 and 2.82 ångström respectively, in addition to its binding to the functional valine 279, 283, and isoleucine 456 residues through the hydrophobic alkyl and pi-alkyl bond at the distance of 5.09 ångström, average distance of 2.58 ångström, and bond distance of 4.69 ångström respectively (Figure 6C; 4). The compound also binds to lysine 287 of the compound through the conventional hydrogen bond at a distance of 2.71 ångström and a rare attractive charge at the distance 4.01 ångström.

Compound TF3 binds to isoleucine 301, leucine 304, valine 283, leucine 452, isoleucine 456 through the hydrophobic alkyl bond at the distances of 5.22, 4.63, 4.55, 4.74, and 4.99 ångström respectively in addition to its binding to lysine 305 through the Pi-alkyl and carbon-hydrogen bond at 5.18 and 2.60 ångström respectively, as well as glutamic acid 455 of the protein through the conventional hydrogen bond, carbon-hydrogen bond, and a salt bridge at the distances of 2.02, 5.46, and 1.94 ångström respectively (Figure 6C; 5).

3.5. Induced fit docking of theaflavins

Globular proteins are known to be not rigid but flexibly alter their side chain conformation (characterized by loops movement or even large domains), upon ligand binding, to fit the optimal ligand pose, in a chain of the process that also involves the target conformational transitions governing the binding-unbinding process (Sherman et al., 2006). This consequently results in significant changes in the free energies of all states along the binding–unbinding pathway and determines appreciable differences in the ligand affinity changes up to multiple hundred folds (Hecht et al., 1992; Hu et al., 2020).

The theaflavin compounds, except the TF1 compound (-7.073 Kcal/mol), exhibited higher Glide GScores of binding than that of desmosterol (-8.144 Kcal/mol), with the TF2A compound showing the highest value, following induced-fit docking of the compounds post-induced-fit docking (Figure 7).

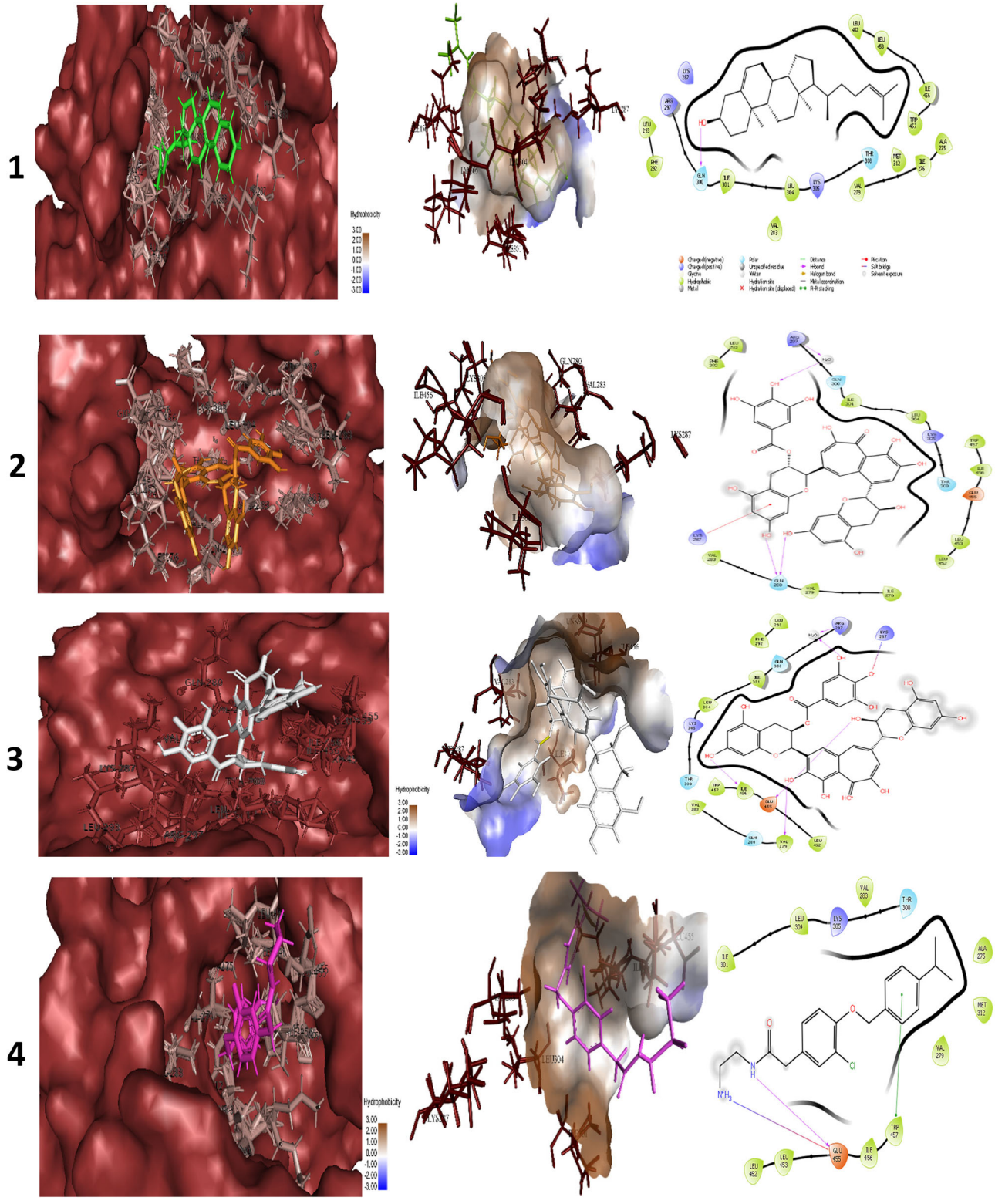


Figure 8. Pocket view (A), pocket hydrophobicity (B) and two-dimensional view (C) of binding interactions between liver X receptor-beta and desmosterol (1), TF1 (2), TF2A (3), TF2B (4) and TF3 (5) following induced fit docking of the compounds.

3.6. Ligand-protein interactions following induced fit docking of theaflavins

The TF2A compound, in common with that of desmosterol, binds to leucine 292, 293, 304, 452, 453, isoleucine 276, 301, 456, tryptophan 457, as well as valine 279 and 283 residues of the protein through the hydrophobic alkyl bond; lysine 305, 287, and arginine 297 through the carbon-hydrogen bond, as well as glutamine 280, 300, and threonine 308 through the conventional hydrogen bond, following induced fit docking analysis in this study (Figure 8C; 2).

The TF2B compound binds to leucine 293, 452, 304, isoleucine 301, 456, tryptophan 457, phenylalanine 292, and

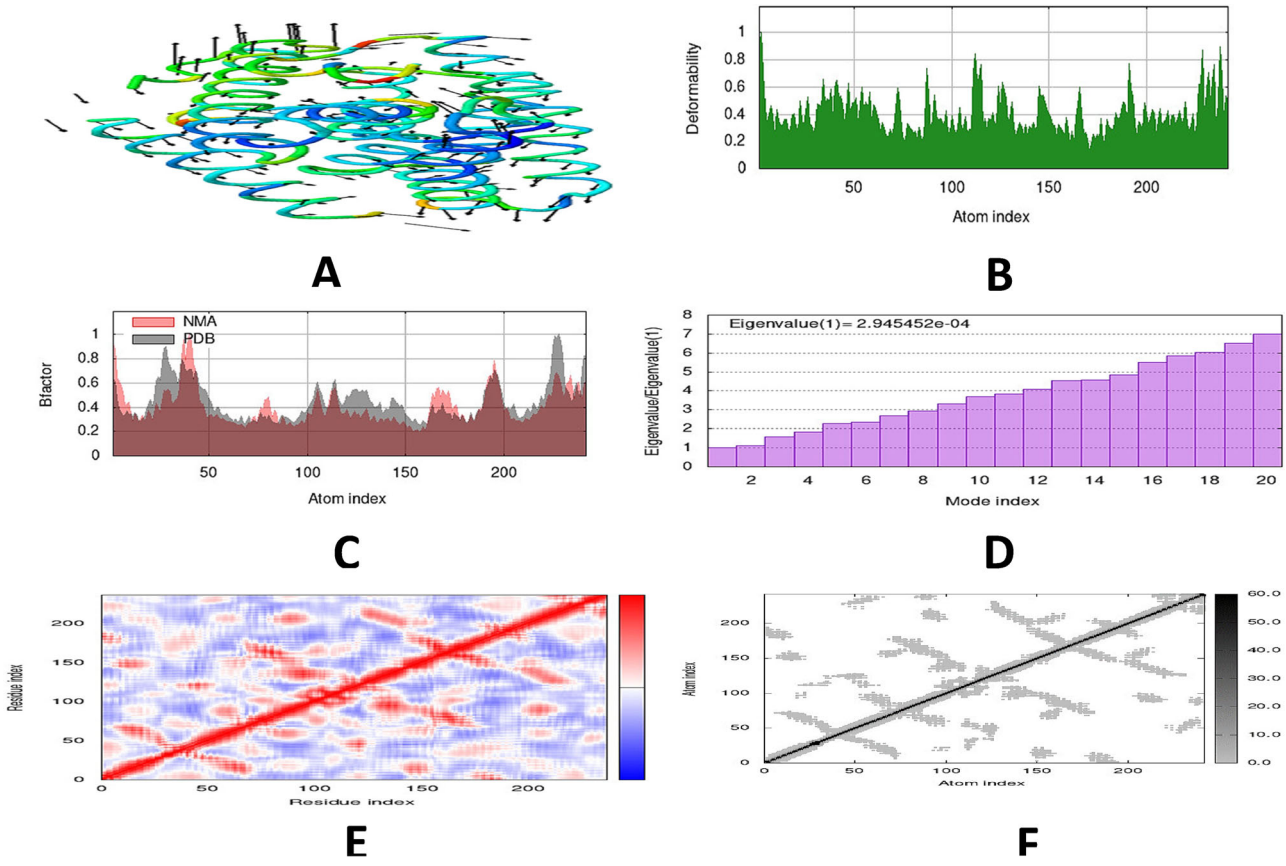


Figure 9. Deformability representation (along with the arrow fields) (A), main chain deformability (B), experimental B-factor (C), eigen values (D), covariance matrix (E), and elastic network model (F) of crystal structure of liver X receptor-beta (6S4T) through normal mode – coarse-grained simulation analysis.

valine 279, 283 of the protein through the hydrophobic alkyl bond; arginine 297, lysine 287, 305 through the conventional hydrogen bond, glutamic acid 455 through the hydrophobic pi-anion bond, as well as glutamine 280, 300, and threonine 308 through the carbon-hydrogen bond (Figure 8C; 3). However, the TF3 compound binds to isoleucine 301, 456, leucine 304, 453, 452 of the Liver X receptor protein through the hydrophobic alkyl bond, lysine 305 through the conventional hydrogen bond; threonine 308 through carbon-hydrogen bond; tryptophan 457 through the Pi-Pi stacking bond; as well as glutamic acid 455 through the hydrophobic Pi-anion bond (Figure 8C; 4).

The ligand-binding cavity of the LXR-beta protein is known to be largely hydrophobic, surrounded by key hydrophobic helical regions including H3, H5, H6, H7, H11 and H12 (Hoerer et al., 2003), while the ligand-induced LXR-beta receptor activation has been shown, by mutational analysis study (Spencer et al., 2001), to be mediated by tryptophan at position 457 (Trp457) (a key residue of the H12 region) through an edge-on hydrophobic interaction of its indole ring (Hoerer et al., 2003). The direct interactions of the theaflavins 2 A, 2B, and 3 with Trp457 post-induced fit docking screens, in this study, may result in stable positioning of activation function 2 (H12) region on top of the H11, H5, and H3 regions, thereby causing subsequent closed-looping on the ligand-binding pocket; a key event that has been inferred from structural data (Xu et al., 2001) as an agonistic conformation of the protein.

3.7. Normal mode – coarse-grained simulation result of liver X receptor-beta apo protein

3.8. Normal mode - coarse grained simulation result of liver X receptor-beta following induced fit docking

The normal mode analysis helps simulate the collective harmonic oscillating motions, closely related to functional motions, of both the unbound (Figure 9) and bound protein (Figure 10) based on harmonic approximation around a local minimum at extended timescales (Dykeman & Sankey, 2010), while its resultant low eigenvalues (2.945452e-^{04}) (Figures 9D and 10D) and deformability values at each of its amino acid residues (Figures 9A, 10A and 9B, 10B) revealed the orthogonal flexibility and high motion stiffness of the protein in both the bound and unbound forms. The deformability values of both the bound and unbound protein in this study, which relies on the singular distortion of each residue (characterizing the chain hinges) indicate that the protein, based on its crystal structure data, is flexible enough for optimal ligand-induced conformation alterations and thermostable enough in dynamic motion for the complex to produce the possible pharmacodynamic effects. The covariance (Figures 9E and 10E) and elastic network (9 F, 10 F) values respectively of both the apo and bound form of the protein also supported this. The covariance values represent the coupling patterns between the pairs of residues with the red, blue, and white colours indicating the correlated, anti-correlated, and uncorrelated motions respectively (López-Blanco et al.,

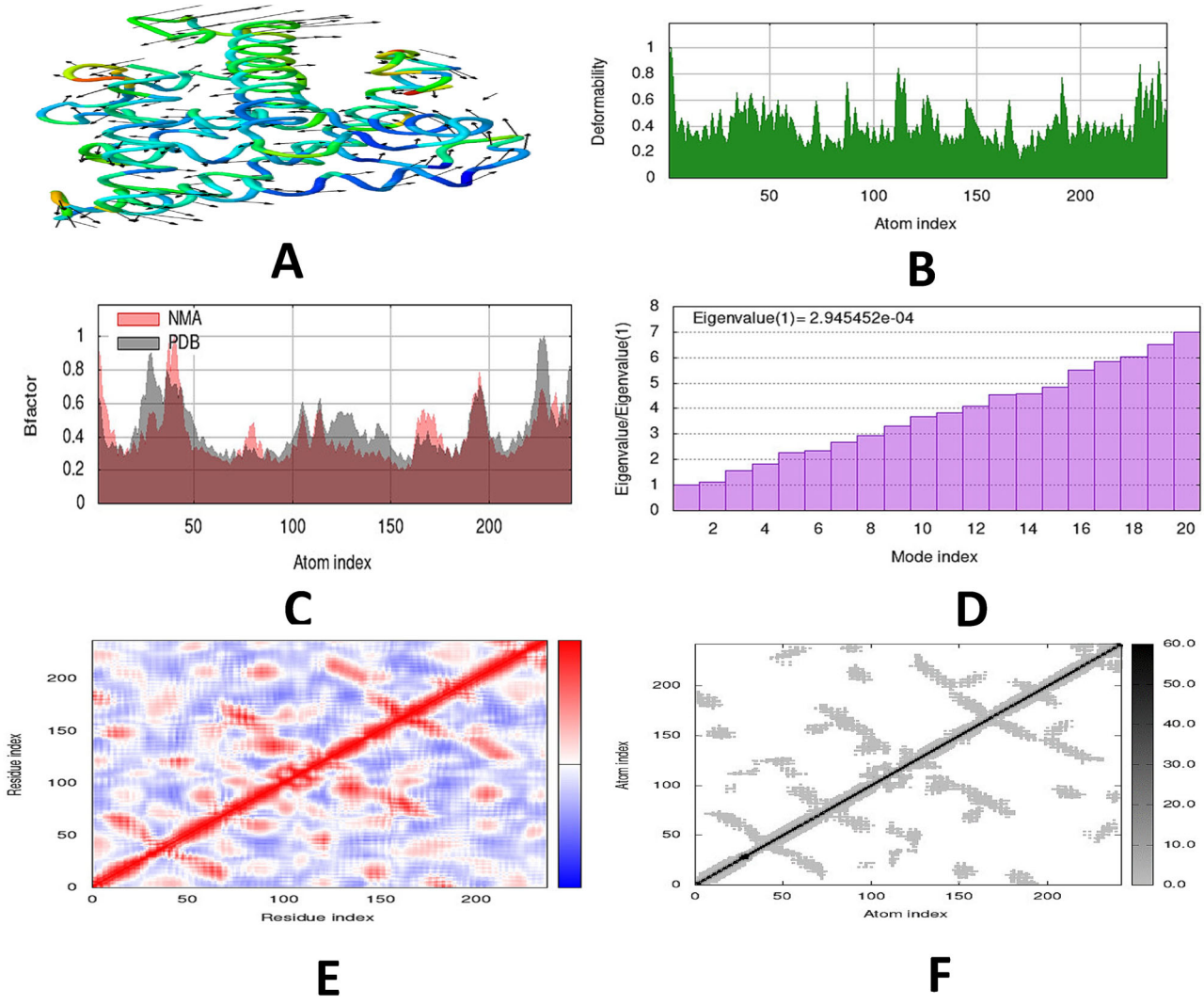


Figure 10. Deformability representation (along with the arrow fields) (A), main chain deformability (B), experimental B-factor (C), eigen values (D), covariance matrix (E), and elastic network model (F) of the extended structure of liver X receptor-beta (6S4T) through normal mode - coarse grained simulation analysis following induced fit docking of compounds.

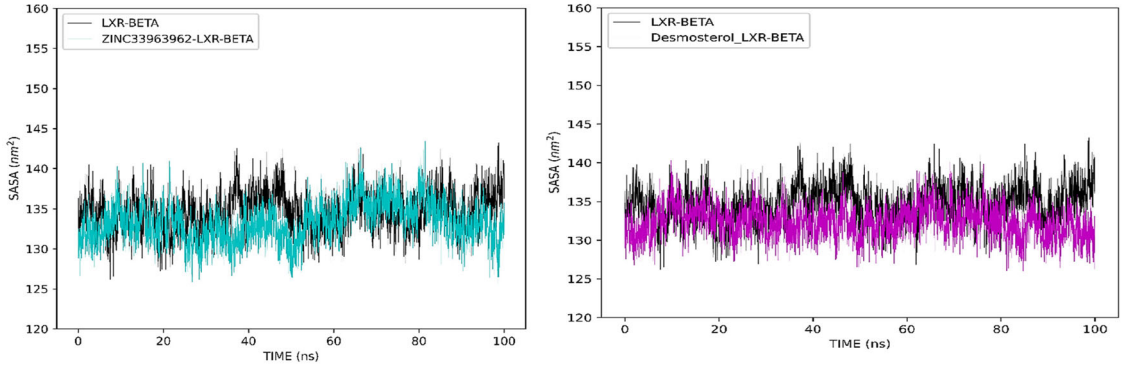


Figure 11. Solvent-accessible surface area (SASA) of theaflavin 2B and desmosterol following 100 nanoseconds molecular dynamics simulations.

2014). The derived experimental B-factors scores (Figures 9C and 10C) also revealed the relative amplitude of atomic displacements around the equilibrium conformation in both the apo and bound form. The simple curved arrows in Figures 9A and 10A depicts the dynamic motions of clustered atoms of the protein and its ligand-bound complex moving together as rigid bodies (Bryden et al., 2012), while the curved arrows in Figure 10 shows the more possible dynamic motions of the bound protein following induced fit docking of theaflavin TF2B compound.

3.9. Molecular dynamics simulations of complexes of compounds with liver X receptor-beta

The solvent-accessible surface area (SASA) value is the rough metric of the degree at which the system reliably mimics the

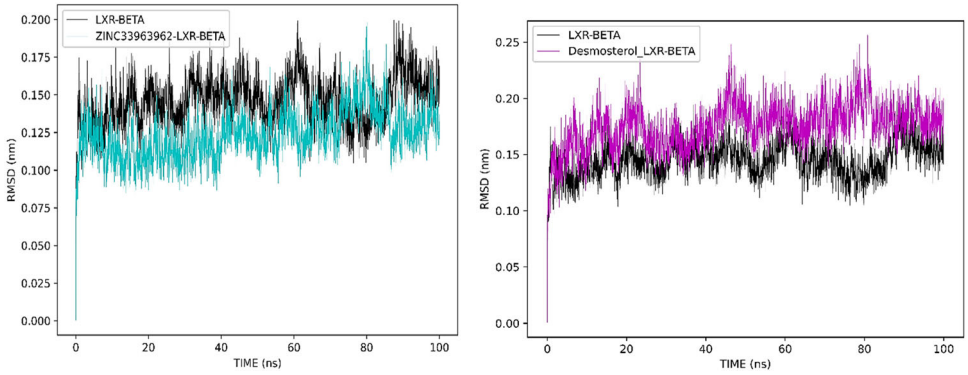


Figure 12. Root mean square deviation of theaflavin 2B and desmosterol following 100 nanoseconds molecular dynamics simulations.

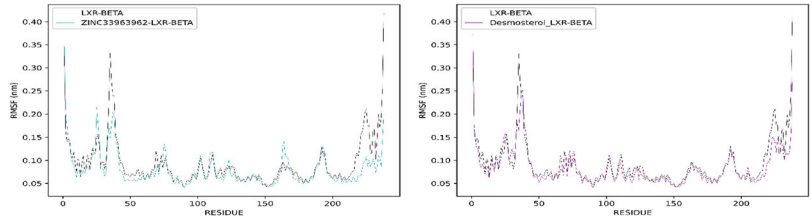


Figure 13. Root mean square fluctuations of theaflavin 2B and desmosterol following 100 nanoseconds molecular dynamics simulations.

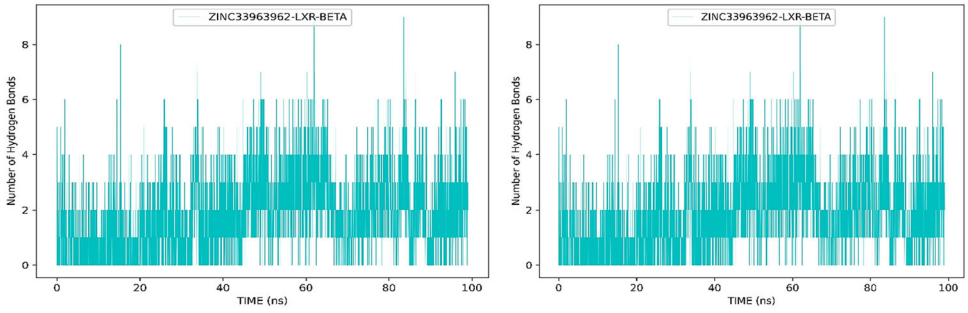


Figure 14. Number of hydrogen bonds of theaflavin 2B and desmosterol following 100 nanoseconds molecular dynamics simulations.

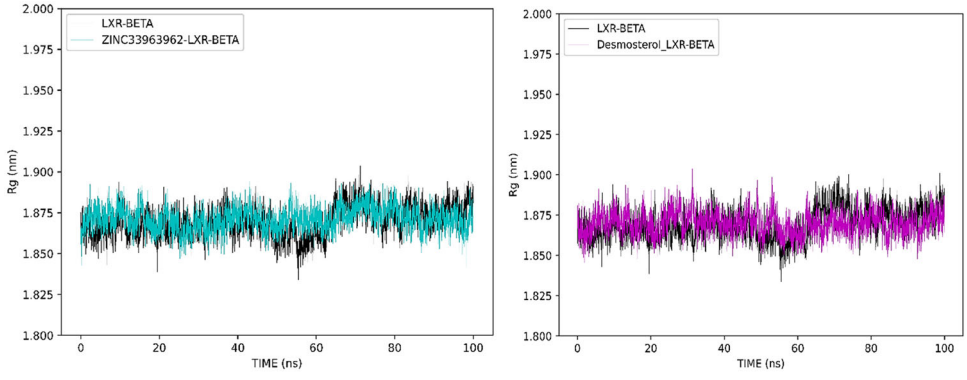


Figure 15. Radius of gyration of theaflavin 2B and desmosterol following 100 nanoseconds molecular dynamics simulations.

internal milieu of the fluidic biological environment during the simulation process, through the accessibility of the surface area of the molecules to solvent (Boyenle et al., 2022; Hikmawati et al., 2022). The mean SASA values (Figure 11) of both the TF2B-LXR-beta complex and that of the standard revealed stable and consistent interaction of both the TF2B compound and desmosterol with the solvent throughout the entire simulation, as well as consistent stability of both protein-ligand complexes.

The root mean square deviation (RMSD) is the average change in displacement of the frame of the protein-ligand complex atoms with respect to the reference frame that is, by default, the first frame at 0 secs. The simulation result of this study revealed the conformational fluctuations of the LXR-beta protein within the range of 1 Å to 1.75 Å (Figure 12) which falls within the simulation of some thermal average structures with the acceptability of changes of the order of 1 Å to 3 Å for most globular proteins. There were

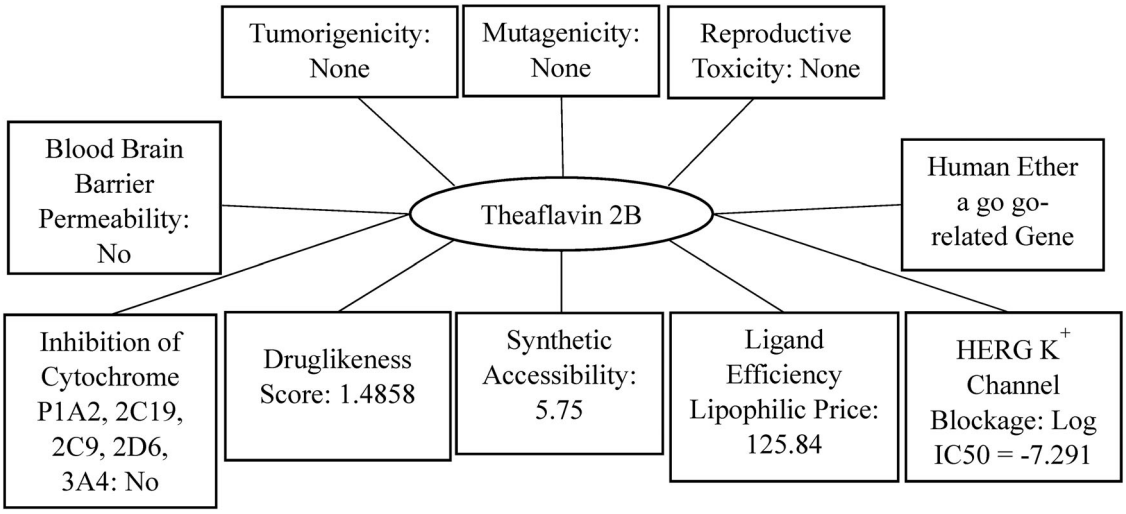


Figure 16. Toxicity, druglikeness, and synthetic accessibility values of theaflavin 2B.

marginally higher deviations in the RMSD value of desmosterol at 80 ns when compared with the slight deviation of the RMSD value of TF2B at around 62 ns, thereby indicating the TF2B compound binds more stably to the protein and its binding pocket and equilibrate throughout the entire 100 ns when compared with that of desmosterol.

The root mean square fluctuations of the protein residue, with respect to each bound ligand, revealed higher local alterations in the protein chain when bound to TF2B compound which is indicated by the various peaks on the residues at positions 25, 75, 60-70, 100-110, 150-175, and 200-250 in comparison with that of the desmosterol-LXR-beta complex showing the various changes with the corresponding peaks on the residues at positions 25, 30-40, 220-250 (Figure 13). These indicate relatively higher flexibility of the residues in the protein and its active site when bound to the TF2B compound than in the Desmosterol-Liver X receptor-beta complex.

The hydrogen bond plays critical role in drug binding to protein, due to its high influence on the specificity, absorption, and metabolism of the drug (Al-Karmalawy et al., 2021; Iman et al., 2015). The TF2B compound in this study formed relatively higher hydrogen bonds to the protein that of the desmosterol (Figure 14) and may have partly contributed to the observed relatively higher stability and equilibration of the TF2B to the protein and its binding pocket, thereby revealing the consistent ability of the compound to maintain hydrogen bond interactions throughout the entire simulation and the relatively higher degree of interaction of the compound with liver X receptor-beta protein; an indicator of high modulatory potential of the compound on the protein.

The radius of gyration is a measure of the compactness and size of the drug-protein complex; a critical component of the functional reliability and, in consequence, efficacy of chemical space of the drug in the living system (Attitalla & Saad, 2017; Singh et al., 2013). The radius of gyration of both the TF2B-LXR-beta complex and desmosterol-LXR-beta complex were approximately constant, within the range of 1.850 – 1.875 nm (Figure 15), and supports the observed overall stability of both complexes throughout the entire 100 ns simulation.

3.10. Absorption, distribution, metabolism, and toxicity of theaflavin TF2B

The theaflavin TF2B compound showed no blood-brain barrier permeability, thereby revealing the non-neurotoxic potential of the compound (Figure 16), unlike most developed LXR-beta agonists that are known to exhibit neurotoxicity; a major limitation of currently developed LXR-beta agonists.

The toxicity evaluation of TF2B compound, over the DataWarrior v5.5.0 algorithm, revealed that it has no tumorigenic, mutagenic, reproductive toxicity potential as well as a weak inhibitory potential (probability of 0.9918) (Figure 16) against human ether a go go-related gene, a critical cardiotoxicity evaluation of compounds. It showed no inhibitory potential against the major cytochrome-containing metabolic enzymes such as cytochrome P1A2, 2C19, 2C9, 2D6, and 3A4; possesses a positive drug-likeness score of 1.4858 and ligand efficiency lipophilic price (LELP) of 125.84 (based on the algorithm implemented within Osiris DataWarrior version 5.5.0), thereby presenting its drug-like features (calculated based on its drug-likeness, water-octanol coefficient, solubility values, molecular weight, as well as toxicity risks) within the range of current FDA-approved drugs (Richter et al., 2017), and it is easily synthesized for further validation in *in vitro* high throughput screening against LXR-beta protein.

4. Conclusion

Cardiovascular diseases and cancer are the first two leading causes of global deaths with shared aetiologies and mechanisms including hypercholesterolemia, while the low activity levels of LXR-beta have been established at the intersection of both. The *in silico* molecular modeling of identified theaflavins in black tea, widely reported for its hypocholesterolaemic effect, revealed theaflavin TF2B as a putatively stable and effective modulatory agent of LXR-beta following induced fit docking and simulations in this study. There is a need, however, for further validation of these findings in *in vitro* high throughput screens and *in vivo* models.

Nevertheless, this indicates that theaflavin-3′-gallate (theaflavin TF2B) is possibly responsible for the widely observed hypocholesterolaemic effect in black tea and that modulation of LXR-beta activity is a probable mechanism involved. This may have a profound impact on the effort to develop novel, safe, and stably potent drug compounds and supplements for the supportive treatment of cardiovascular diseases and their associated cancers.

Disclosure statement

No potential conflict of interest was reported by the authors.

Funding

The authors of this research appreciate the support of the University of Groningen Peregrine, The Netherlands, for the provision of part of the computational resources employed for the study.

ORCID

Haruna I. Umar http://orcid.org/0000-0001-9427-9804
Mutiu A. Alabi http://orcid.org/0000-0002-2236-9795

Author contributions

Conceived and conceptualized: T.O.A.; study design: T.O.A., H.I.U., and A.U.D.; methodology: T.O.A., A.U.D., and A.N.; resources: T.O.A., A.U.D., H.I.U., A.N., M.A.A., W.O.J., A.A., O.O.A.; writing—original draft preparation: T.O.A.; writing—critical review, revised version, and re-editing: T.O.A., A.U.D., H.I.U., A.N., M.A.A., W.O.J., A.A., O.O.A., J.O.B., O.S.O., O.A.M.; project administration: T.O.A. and H.I.U.; principal investigator: T.O.A. All authors have read and agreed to the published version of the manuscript.

References

Al-Karmalawy, A. A., Dahab, M. A., Metwaly, A. M., Elhady, S. S., Elkaeed, E. B., Eissa, I. H., & Darwish, K. M. (2021). Molecular docking and dynamics simulation revealed the potential inhibitory activity of ACEIs against SARS-CoV-2 targeting the hACE2 receptor. *Frontiers in Chemistry*, *9*, 661230). https://doi.org/10.3389/fchem.2021.661230

Attitalla, I. H., & Saad, E. I. F. (2017). Molecular dynamic simulation and an inhibitor prediction of PI3K (P110α) subunit mutant protein structured model as a potential drug target for cancer. *Journal Oncology*, *1*(1), 7. www.imedpub.com/research-journal-oncology).

Bełtowski, J. (2008). Liver X receptors (LXR) as therapeutic targets in dyslipidaemia. *Cardiovascular Therapeutics*, *26*(4), 297–316). https://doi.org/10.1111/j.1755-5922.2008.00062.x

Bovenga, F., Sabba, C., & Moschetta, A. (2015). Uncoupling nuclear receptor LXR and cholesterol metabolism in cancer. *Cell Metabolism*, *21*(4), 517–526. https://doi.org/10.1016/j.cmet.2015.03.002

Boyenle, I. D., Adelusi, T. I., Ogunlana, A. T., Oluwabusola, R. A., Ibrahim, N. O., Tolulope, A., Okikiola, O. S., Adetunji, B. L., Abioye, I. O., & Oyedele, A. K. (2022). Consensus scoring-based virtual screening and molecular dynamics simulation of some TNF-alpha inhibitors. *Informatics in Medicine Unlocked*, *28*, 100833). https://doi.org/10.1016/j.imu.2021.100833

Bradley, M. N., & Tontonoz, P. (2005). LXR: A nuclear receptor target for cardiovascular disease? *Drug Discovery Today: Therapeutic Strategies*, *2*(2), 97–103). https://doi.org/10.1016/j.ddstr.2005.05.018

Bryden, A., Phillips, G., & Gleicher, M. (2012). Automated illustration of molecular flexibility. *IEEE Transactions on Visualization and Computer Graphics*, *18*(1), 132–145. https://doi.org/10.1109/TVCG.2010.250

Chen, Y. (2015). Beware of docking! *Trends in Pharmacological Sciences*, *36*(2), 78–95. https://doi.org/10.1016/j.tips.2014.12.001

Chu, K., Miyazaki, M., Man, W. C., & Ntambi, J. M. (2006). Stearoyl-coenzyme A desaturase 1 deficiency protects against hypertriglyceridemia and increases plasma high-density lipoprotein cholesterol induced by liver X receptor activation. *Molecular and Cellular Biology*, *26*(18), 6786–6798. https://doi.org/10.1128/MCB.00077-06

Dykeman, E. C., & Sankey, O. F. (2010). Normal mode analysis and applications in biological physics. *Journal of Physics: Condensed Matter*, *22*(42), 423202. https://doi.org/10.1088/0953-8984/22/42/423202

Groot, P. H. E., Pearce, N. J., Yates, J. W., Stocker, C., Sauermelch, C., Doe, C. P., Willette, R. N., Olzinski, A., Peters, T., d'Epagnier, D., Morasco, K. O., Krawiec, J. A., Webb, C. L., Aravindhan, K., Jucker, B., Burgert, M., Ma, C., Marino, J. P., Collins, J. L., … Jaye, M. (2005). Synthetic LXR agonists increase LDL in CETP species. *Journal of Lipid Research*, *46*(10), 2182–2191.

Hecht, H. J., Szardenings, M., Collins, J., & Schomburg, D. (1992). Three-dimensional structure of a recombinant variant of human pancreatic secretory trypsin inhibitor (Kazal type). *Journal of Molecular Biology*, *225*(4), 1095–1103. https://doi.org/10.1016/0022-2836(92)90107-u

Hess, L. A., & van Der, S. (2021). *GROMACS 2021 manual*. GROMACS Development Team. https://doi.org/10.5281/ZENODO.4457591

Hikmawati, D., Fakih, T. M., Sutedja, E., Dwiyana, R. F., Atik, N., & Ramadhan, D. S. F. (2022). Pharmacophore-guided virtual screening and dynamic simulation of kallikrein-5 inhibitor: Discovery of potential molecules for rosacea therapy. *Informatics in Medicine Unlocked*, *28*, 100844). https://doi.org/10.1016/j.imu.2022.100844

Hoerer, S., Schmid, A., Heckel, A., Budzinski, R.-M., & Nar, H. (2003). Crystal structure of the human liver X receptor-beta. ligand-binding domain in complex with a synthetic agonist. *Journal of Molecular Biology*, *334*(5), 853–861). https://doi.org/10.1016/j.jmb.2003.10.033

Hu, G., Li, H., Xu, S., & Wang, J. J. I. (2020). Ligand binding mechanism and its relationship with conformational changes in adenine riboswitch. *International Journal of Molecular Sciences*, *21*(6), 1926. https://doi.org/10.3390/ijms21061926

Iman, M., Saadabadi, A., & Davood, A. (2015). Molecular docking analysis and molecular dynamics simulation study of ameltolide analogous as a sodium channel blocker. *Turkish Journal of Chemistry*, *39*, 306–316). https://doi.org/10.3906/kim-1402-37

Jin, D., Xu, Y., Mei, X., Meng, Q., Gao, Y., Li, B., & Tu, Y. (2013). Antiobesity and lipid lowering effects of theaflavins on high-fat diet-induced obese rats. *Journal of Functional Foods*, *5*(3), 1142–1150). https://doi.org/10.1016/j.jff.2013.03.011

Ju, X., Huang, P., Chen, M., & Wang, Q. (2017). Liver X receptors as potential targets for cancer therapeutics (review). *Oncology Letters*, *14*(6), 7676–7680. https://doi.org/10.3892/ol.2017.7259

Kick, E. K., Busch, B. B., Martin, R., Stevens, W. C., Bollu, V., Xie, Y., Boren, B. C., Nyman, M. C., Nanao, M. H., Nguyen, L., Plonowski, A., Schulman, I. G., Yan, G., Zhang, H., Hou, X., Valente, M. N., Narayanan, R., Behnia, K., Rodrigues, A. D., … Mohan, R. (2016). Discovery of highly potent liver X receptor β agonists. *ACS Medicinal Chemistry Letters*, *7*(12), 1207–1212). https://doi.org/10.1021/acsmedchemlett.6b00234

Kuo, K.-L., Weng, M.-S., Chiang, C.-T., Tsai, Y.-J., Lin-Shiau, S.-Y., & Lin, J.-K. (2005). Comparative studies on the hypolipidemic and growth suppressive effects of oolong, black, Pu-Erh, and green tea leaves in rats. *Journal of Agricultural and Food Chemistry*, *53*(2), 480–489.

Lin, C. L., Huang, H. C., & Lin, J. K. (2007). Theaflavins attenuate hepatic lipid accumulation through activating AMPK in human HepG2 Cells. *Journal of Lipid Research*, *48*(11), 2334–2343. https://doi.org/10.1194/jlr.M700128-JLR200

Lin, C. Y., & Gustafsson, J. A. (2015). Targeting liver X receptors in cancer therapeutics. *Nature Reviews. Cancer*, *15*(4), 216-–224. https://doi.org/10.1038/nrc3912

Long, H., Guo, X., Qiao, S., & Huang, Q. (2018). Tumor LXR Expression is a prognostic marker for patients with hepatocellular carcinoma. *Pathology Oncology Research : POR*, *24*(2), 339–344. https://doi.org/10.1007/s12253-017-0249-8

López-Blanco, J. R., Aliaga, J. I., Quintana-Ortí, E. S., & Chacón, P. (2014). iMODS: Internal coordinates normal mode analysis server. *Nucleic Acids Research*, *42*, W271–W276). https://doi.org/10.1093/nar/gku339

Lund, E. G., Menke, J. G., & Sparrow, C. P. (2003). Liver X receptor agonists as potential therapeutic agents for dyslipidemia and atherosclerosis. *Arteriosclerosis, Thrombosis, and Vascular Biology*, *23*(7), 1169–1177). https://doi.org/10.1161/01.ATV.0000056743.42348.59

Maron, D. J., Lu, G. P., Cai, N. S., Wu, Z. G., Li, Y. H., Chen, H., Zhu, J. Q., Jin, X. J., Wouters, B. C., & Zhao, J. (2003). Cholesterol-lowering effect of a theaflavin-enriched green tea extract: A randomized controlled trial. *Archives of Internal Medicine*, *163*(12), 1448–1453. https://doi.org/10.1001/archinte.163.12.1448

Morrow, M. P., Grant, A., Mujawar, Z., Dubrovsky, L., Pushkarsky, T., Kiselyeva, Y., Jennelle, L., Mukhamedova, N., Remaley, A. T., Kashanchi, F., Sviridov, D., & Bukrinsky, M. (2010). Stimulation of the liver X receptor pathway inhibits HIV-1 replication via induction of ATP-binding cassette transporter A1. *Molecular Pharmacology*, *78*(2), 215–225. https://doi.org/10.1124/mol.110.065029

Nabuurs, S. B., Wagener, M., & de Vlieg, J. (2007). Flexible approach to induced fit docking. *Journal of Medicinal Chemistry*, *50*(26), 6507–6518. https://doi.org/10.1021/jm070593pCCC:$37.00).

Nguyen-Vu, T., Vedin, L., Liu, K., Jonsson, P., Lin, J. Z., Candelaria, N. R., Candelaria, L. P., Addanki, S., Williams, C., Gustafsson, J., Steffensen, K. R., & Lin, C. (2013). Liver X receptor ligands disrupt breast cancer cell proliferation through an E2F-mediated mechanism. *Breast Cancer Research : BCR*, *15*(3), R51). https://doi.org/10.1186/bcr3443

Noghero, A., Perino, A., Seano, G., Saglio, E., Lo Sasso, G., Veglio, F., Primo, L., Hirsch, E., Bussolino, F., & Morello, F. (2012). Liver X receptor activation reduces angiogenesis by impairing lipid raft localization and signaling of vascular endothelial growth factor receptor-2. *Arteriosclerosis, Thrombosis, and Vascular Biology*, *32*(9), 2280–2288.

Patrick, G. L. (2013). *An introduction to medicinal chemistry* (pp. 189–191). Oxford University Press.

Ramadan, G., El-Beih, N. M., & Abd El-Ghffar, E. A. (2009). Modulatory effects of black vs green tea aqueous extract on hyperglycaemia, hyperlipidaemia and liver dysfunction in diabetic and obese rat models. *British Journal of Nutrition*, *102*(11), 1611–1619. https://doi.org/10.1017/S000711450999208X

Repa, J. J., Berge, K. E., Pomajzl, C., Richardson, J. A., Hobbs, H., & Mangelsdorf, D. J. (2002). Regulation of ATP-binding cassette sterol transporters ABCG5 and ABCG8 by the liver X receptors alpha and beta. *Journal of Biological Chemistry*, *277*(21), 18793–18800. https://doi.org/10.1074/jbc.M109927200

Repa, J. J., Liang, G., Ou, J., Bashmakov, Y., Lobaccaro, J. M., Shimomura, I., Shan, B., Brown, M. S., Goldstein, J. L., & Mangelsdorf, D. J. (2000). Regulation of mouse sterol regulatory element-binding protein-1C Gene (SREBP-1c) by oxysterol receptors, LXR-alpha and LXR-beta. *Genes & Development*, *14*(22), 2819–2830. https://doi.org/10.1101/gad.844900

Richter, M. F., Drown, B. S., Riley, A. P., Garcia, A., Shirai, T., Svec, R. L., & Hergenrother, P. J. (2017). Predictive compound accumulation rules yield a broad-spectrum antibiotic. *Nature*, *545*(7654), 299–304. https://doi.org/10.1038/nature22308

Schulman, I. G. (2017). Liver X receptors link lipid metabolism and inflammation. *FEBS Letters*, *591*(19), 2978–2991. https://doi.org/10.1002/1873-3468.12702)

Shao, W., Kuhn, C., Mayr, D., Ditsch, N., Kailuwait, M., Wolf, V., Harbeck, N., Mahner, S., Jeschke, U., Cavaillès, V., & Sixou, S. (2021). Cytoplasmic LXR expression is an independent marker of poor prognosis for patients with early-stage primary breast cancer. *Journal of Cancer Research and Clinical Oncology*, *147*(9), 2535–2544. ·). https://doi.org/10.1007/s00432-021-03670-y

Shao, W., Zhua, W., Lin, J., Luo, M., Lin, Z., Lu, L., Jia, H., Qin, L., Lu, M., & Chen, J. (2020). Liver X receptor agonism sensitizes a subset of hepatocellular carcinoma to sorafenib by dual-inhibiting MET and EGFR. *Journal of Cancer Research and Clinical Oncology*, *22*(1), 1–9.

Sherman, W., Beard, H. S., & Farid, R. (2006). Use of an induced fit receptor structure in virtual screening. *Chemical Biology & Drug Design*, *67*(1), 83–84). https://doi.org/10.1111/j.1747-0285.2005.00327.x

Singh, S., Sablok, G., Farmer, R., Singh, A. K., Gautam, B., & Kumar, S. (2013). Molecular dynamic simulation and inhibitor prediction of cysteine synthase structured model as a potential drug target for trichomoniasis. *BioMed Research International*, *2013*, 390920. https://doi.org/10.1155/2013/390920

Spencer, T. A., Li, D., Russel, J. S., Collins, J. L., Bledsoe, R. K., Consler, T. G., Moore, L. B., Galardi, C. M., McKee, D. D., Moore, J. T., Watson, M. A., Parks, D. J., Lambert, M. H., & Willson, T. M. (2001). Pharmacophore analysis of the nuclear oxysterol receptor LXR-alpha. *Journal of Medicinal Chemistry*, *44*(6), 886–897. https://doi.org/10.1021/jm0004749

Trautwein, E. A., Du, Y., Meynen, E., Yan, X., Wen, Y., Wang, H., & Molhuizen, H. O. F. (2010). Purified black tea theaflavins and theaflavins/catechin supplements did not affect serum lipids in healthy individuals with mildly to moderately elevated cholesterol concentrations. *European Journal of Nutrition*, *49*(1), 27–35). https://doi.org/10.1007/s00394-009-0045-7

Vázquez-Salgado, A. M., Preziosi, M. E., Yin, D., Holczbauer, A., Zahm, A. M., , Erez, N., Kieckhaefer, J., Ackerman, D., Gade, T. P., Kaestner, K. H., & Wangensteen, K. J. (2019). *In vivo* screen identifies LXR agonism potentiates sorafenib killing of hepatocellular carcinoma. *ghAdvances*, *1*(5), 905–908. https://doi.org/10.1016/j.gastha.2022.05.014

Vanommeslaeghe, K., Hatcher, E., Acharya, C., Kundu, S., Zhong, S., Shim, J., Darian, E., Guvench, O., Lopes, P., Vorobyov, I., & Mackerell, A. D. (2010). CHARMM general force field: A force field for drug-like molecules compatible with the CHARMM All-atom additive biological force fields. *Journal of Computational Chemistry*, *31*(4), 671–690). https://doi.org/10.1002/JCC.21367

Vedin, L., Lewandowski, S. A., Parini, P., Gustafsson, J., & Steffensen, K. R. (2009). The oxysterol receptor LXR inhibits proliferation of human breast cancer cells. *Carcinogenesis*, *30*(4), 575–579). https://doi.org/10.1093/carcin/bgp029

Viennois, E., Pommier, A. J. C., Mouzat, K., Oumeddour, A., El Hajjaji, F., Dufour, J., Caira, F., Volle, D. H., Baron, S., & Lobaccaro, J. A. (2011). Targeting liver X receptors in human health: Deadlock or promising trail? *Expert Opinion on Therapeutic Targets*, *15*(2), 219–232. https://doi.org/10.1517/14728222.2011.547853

Villa, G. R., Hulce, J. J., Zanca, C., Bi, J., Ikegami, S., Cahill, G. L., Gu, Y., Lum, K. M., Masui, K., Yang, H., Rong, X., Hong, C., Turner, K. M., Liu, F., Hon, G. C., Jenkins, D., Martini, M., Armando, A. M., Quehenberger, O., … Mischel, P. S. (2016). An LXR-cholesterol axis creates a metabolic co-dependency for brain cancers. *Cancer Cell*, *30*(5), 683–693. https://doi.org/10.1016/j.ccell.2016.09.008

Wang, Q., Feng, F., Wang, J., Ren, M., Shi, Z., Mao, X., Zhang, H., & Ju, X. (2019). Liver X receptor activation reduces gastric cancer cell proliferation by suppressing WNT signalling via LXR-β relocalization. *Journal of Cellular and Molecular Medicine*, *23*(2), 789-–797). https://doi.org/10.1111/jcmm.13974

Xu, H. E., Lambert, M. H., Montana, V. G., Plunket, K. D., Moore, L. B., Collins, J. L., Oplinger, J. A., Kliewer, S. A., Gampe, R. T., McKee, D. D., Moore, J. T., & Willson, T. M. (2001). Structural determinants of ligand binding selectivity between the peroxisome proliferator-activated receptors. *Proceedings of the National Academy of Sciences of the United States of America*, *98*(24), 13919–13924. https://doi.org/10.1073/pnas.241410198

Yu, W., He, X., Vanommeslaeghe, K., & MacKerell, A. D. (2012). Extension of the CHARMM general force field to sulfonyl-containing compounds and its utility in biomolecular simulations. *Journal of Computational Chemistry*, *33*(31), 2451–2468. https://doi.org/10.1002/JCC.23067

Zeng, J., Wu, Y., Liao, Q., Li, L., Chen, X., & Chen, X. (2012). Liver X receptors agonists impede hepatitis C virus infection in an IDOl-dependent manner. *Antiviral Research*, *95*(3), 245–256. https://doi.org/10.1016/j.antiviral.2012.06.004

Zhao, C., & Dahlman-Wright, K. (2010). Liver X receptor in cholesterol metabolism. *The Journal of Endocrinology*, *204*(3), 233–240). https://doi.org/10.1677/JOE-09-0271